

Quasi-perpendicular shock acceleration and TDE radio flares

SIYAO XU¹

¹*Institute for Advanced Study, 1 Einstein Drive, Princeton, NJ 08540, USA; sxu@ias.edu*^a

ABSTRACT

Delayed radio flares of optical tidal disruption events (TDEs) indicate the existence of non-relativistic outflows accompanying TDEs. The interaction of TDE outflows with the surrounding circumnuclear medium creates quasi-perpendicular shocks in the presence of toroidal magnetic fields. Because of the large shock obliquity and large outflow velocity, we find that the shock acceleration induced by TDE outflows generally leads to a steep particle energy spectrum, with the power-law index significantly larger than the “universal” index for a parallel shock. The measured synchrotron spectral indices of recently detected TDE radio flares are consistent with our theoretical expectation. It suggests that the particle acceleration at quasi-perpendicular shocks can be the general acceleration mechanism accounting for the delayed radio emission of TDEs.

1. INTRODUCTION

Stars in galactic nuclei can be tidally disrupted by a central super-massive black hole (SMBH) (Rees 1988). The resulting tidal disruption events (TDEs) produce transient emission at optical/UV and X-ray bands (Saxton et al. 2020; van Velzen et al. 2020). They also eject sub-relativistic outflows, as indicated by the radio flares detected several months or years after the stellar disruption (Alexander et al. 2020; Matsumoto & Piran 2021). The delayed radio flares are believed as the synchrotron emission from accelerated electrons when a TDE outflow interacts with the circumnuclear medium (CNM) surrounding the SMBH. The observed synchrotron spectra provide constraints on the outflow properties and CNM density (Matsumoto & Piran 2021). As non-relativistic outflows can be ubiquitous in TDEs (Alexander et al. 2016), understanding the associated fundamental acceleration process is important not only for interpreting the follow-up radio observations, but also for determining whether TDE outflows are a possible source of high-energy cosmic rays and neutrinos (Murase et al. 2020b; Stein et al. 2021; Wu et al. 2021).

The outflow-CNM interaction gives rise to (bow) shocks in the CNM (Matsumoto & Piran 2021). Shock acceleration and the energy spectrum of accelerated particles are highly sensitive to the obliquity angle between the upstream magnetic field and local shock normal (Jokipii 1987; Naito & Takahara 1995; Bell et al. 2011; Xu & Lazarian 2022). In the case of dominant toroidal magnetic field in the CNM (Silant'ev et al. 2013; Piotrovich et al. 2017), the shocks driven by TDE outflows are expected to be predominantly quasi-perpendicular with large obliquities.

Particle acceleration at quasi-perpendicular shocks is frequently considered for interplanetary shocks, which are mainly quasi-perpendicular at 1 AU with respect to the Parker spiral magnetic field in the solar wind (Guo et al. 2021). Compared with quasi-parallel shocks, quasi-

perpendicular shocks have a much higher acceleration efficiency (Jokipii 1987; Xu & Lazarian 2022). Thus they tend to dominate the particle acceleration when there is a variation of shock obliquities (Decker 1988; Fulbright & Reynolds 1990; West et al. 2017; Bell et al. 2011). Xu & Lazarian (2022) (hereafter XL22) studied the acceleration at supernova shocks propagating through inhomogeneous media and found that acceleration by quasi-perpendicular shocks can well explain the steep radio synchrotron spectra commonly seen in young supernova remnants (see e.g., Maeda 2013 for an alternative explanation). The importance of particle acceleration at the quasi-perpendicular shocks driven by TDE outflows for interpreting their synchrotron spectra has not been addressed.

The increasing number of radio TDEs detected in recent years motives this study on the origin of accelerated electrons accounting for the radio synchrotron emission. In this letter, we will investigate the particle acceleration process at shocks driven by TDE outflows and provide predictions for upcoming observations on synchrotron spectra of TDE radio flares. In Section 2, we describe the magnetic field geometry and shock obliquity. In Section 3, we analyze the obliquity dependence of shock acceleration and particle energy spectrum. In Section 4, we compare the theoretical expectation with available measurements on synchrotron spectral slopes of radio TDEs. Discussion and main conclusions are provided in Sections 5 and 6.

2. QUASI-PERPENDICULAR SHOCKS DRIVEN BY TDE OUTFLOWS

Possible outflows accompanying TDEs include spherical disk winds from super-Eddington accretion disks, unbound stellar debris, and Newtonian jets (Matsumoto & Piran 2021). When a sub-relativistic outflow launched by a TDE interacts with the CNM and the clouds around SMBHs (Christopher et al. 2005; Ciurlo et al. 2020), (bow) shocks form in the CNM and around the clouds (Mou et al. 2022).

As estimated from polarimetric observations (Silant'ev et al. 2013; Piotrovich et al. 2017), the magnetic fields in the

^a Hubble Fellow

broad line region (BLR) of active galactic nuclei (AGN) are dominated by the toroidal component due to the differential rotation in the accretion disk (Bonanno & Urpin 2007), with a typical strength of ~ 10 G. As SMBHs actively grow during the AGN phase, it can be naturally expected that many SMBHs still have relic toroidal magnetic fields around them when they are in the quiescent phase. One example is Sagittarius A* (Sgr A*), which is currently quiescent but was recently active (Nicastrò et al. 2016). The detailed mapping of the magnetic fields in the central parsec of the Galaxy using dust polarization (Roche et al. 2018) and the Velocity Gradient Technique (Hu et al. 2022b) reveals a significant toroidal component of magnetic fields around Sgr A*. The magnetic fields are associated with the circumnuclear gas that is likely spiraling into the SMBH (Roche et al. 2018). More evidence on toroidal magnetic fields around SMBHs requires more magnetic field measurements in galaxy centers (Hu et al. 2022a).

Given the toroidal geometry of the magnetic fields, irrespective of the specific outflow origin, the shocks in the CNM are basically quasi-perpendicular, with the upstream mean magnetic field nearly perpendicular to the shock normal. We illustrate the quasi-perpendicular bow shock around a cloud near an SMBH and the quasi-perpendicular shock expanding isotropically in the CNM in Fig. 1. In the case of the bow shock, the magnetic draping leads to the development of a magnetic precursor and a wide opening angle of the bow shock due to the magnetic tension (Burdiak et al. 2017).

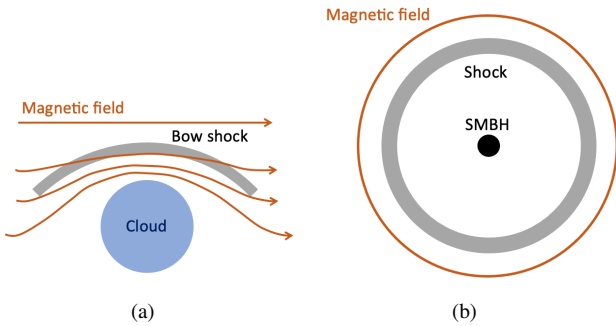


Figure 1. Schematic illustration of quasi-perpendicular shocks driven by TDE outflows in the presence of toroidal magnetic fields in the CNM. (a) A zoom-in of the bow shock around a cloud in the CNM. (b) The shock of a disk wind expanding in the CNM. In both cases, the shock normal is nearly perpendicular to the background mean magnetic field.

3. OBLIQUITY-DEPENDENT PARTICLE SPECTRAL INDEX

At a subluminal oblique shock, due to the shock compression of magnetic fields, particles can be either reflected upstream or transmitted crossing the shock into the downstream region. The particles undergo the shock drift acceleration (SDA) when they drift along the shock surface (Sonnerup 1969; Wu 1984; Armstrong et al. 1985; Ball & Mel-

rose 2001). In the presence of magnetic fluctuations, which can be preexisting or driven by turbulent dynamo (Beresnyak et al. 2009; Drury & Downes 2012; del Valle et al. 2016; Xu & Lazarian 2017) and accelerated particles (Bell 1978, 2004), the particles can repeatedly diffuse across the shock and are accelerated through a combination of SDA and diffusive shock acceleration (DSA) (Jokipii 1982; Decker & Vlahos 1986; Ostrowski 1988; Kirk & Heavens 1989). The energy spectral slope of accelerated particles is determined by the competition between acceleration and loss of particles. As both processes depend on the shock obliquity, the resulting spectral index is also obliquity dependent.

Quasi-parallel shock. We define

$$\beta_1 = \frac{U_1}{c \cos \alpha_1}, \quad \beta_2 = \frac{U_2}{c \cos \alpha_2}, \quad (1)$$

where subscripts $i = 1, 2$ denote the upstream and downstream regions, U_i is the shock speed in the local fluid frame with $U_1 = 4U_2$ for a strong shock considered in this work, c is the light speed, α_i is the angle between the shock normal and the magnetic field, and α_1 is the shock obliquity. At a quasi-parallel shock with a small α_1 and a non-relativistic shock speed $U_{\text{sh}} = U_1$, we are in the limit of a small β_1 .

The power-law index γ of the particle energy spectrum $N(E) \propto E^{-\gamma}$ is

$$\gamma = 1 - \frac{\ln P}{\ln \epsilon}, \quad (2)$$

where E is the particle energy, $\epsilon = 1 + d$, and d is the fractional energy gain per shock crossing cycle. $P = 1 - P_{\text{esp}}$ and P_{esp} are probabilities that a particle returns to and escapes from the acceleration region in each shock crossing. A shallower spectrum (i.e., a smaller γ) is expected at a larger d and a smaller P_{esp} . For instance, the shallowest spectrum with $\gamma = 1$ corresponds to $P_{\text{esp}} = 0$, i.e., no escape of particles. Naturally, the spectrum becomes steep when P_{esp} is large.

In the limit case of a small β_1 for a quasi-parallel shock, we approximately have $d \approx \beta_1$ (XL22) and $P_{\text{esp}} \approx \beta_1$ (Bell 1978), leading to

$$\gamma \approx 1 - \frac{\ln(1 - \beta_1)}{\ln(1 + \beta_1)}. \quad (3)$$

We see that γ approaches 2 at a sufficiently small β_1 . We note that $\gamma = 2$ is the so-called “universal” spectral index for acceleration at a parallel shock, for which only the DSA is at work.

Quasi-perpendicular shock. In a more general case with a large α_1 and a large β_1 , we have a general expression of d (XL22)

$$d = (P_{12} - P_{\text{esp}})(d_{12} + d_{21}) + P_{\text{esp}}d_{12} + P_r d_r, \quad (4)$$

where (Naito & Takahara 1995)

$$P_{\text{esp}} = P_{12} \frac{4\beta_2}{(1 + \beta_2)^2}, \quad (5)$$

P_r and P_{12} are the probabilities of reflection and transmission, and d_r and d_{12} (d_{21}) are the fractional energy gain for reflection and transmission from upstream (downstream) to downstream (upstream). Their expressions are provided in Appendix.

Fig. 2 shows d , P_{esp} (Fig. 2(a)), and γ (Fig. 2(b)) as a function of $\cos \alpha_1$ for sub-relativistic shocks. Both d and P_{esp} increase with obliquity. The significant energy gain at large obliquities, with d even exceeding unity, is mainly contributed by the reflection process in the SDA. The large d also causes a slightly shallower spectrum compared to the quasi-parallel case. Very close to the largest obliquity for a subluminal shock with $\beta_1 \lesssim 1$, almost all particles are transmitted downstream. The lack of reflection causes the drop of d . Meanwhile, P_{esp} approaches unity. As a result, the particle spectrum is drastically steepened, and we see in Fig. 2(b) a large γ for a quasi-perpendicular shock.

Fig. 3 shows d , P_{esp} (Fig. 3(a)), and γ (Fig. 3(b)) as a function of U_{sh} for a quasi-parallel shock with $\alpha_1 = 20^\circ$ and a quasi-perpendicular shock with $\alpha_1 = 72^\circ$. We note that $\alpha_1 = 72^\circ$ corresponds to $\beta_1 \approx 1$ for $U_{\text{sh}} = 0.3c$. Despite the increase of d and P_{esp} with U_{sh} , d and P_{esp} remain small for a quasi-parallel shock. The resulting γ is well described by Eq. (3) at a small U_{sh} , which is around 2 when $\beta_1 \ll 1$ and becomes slightly larger than 2 at a large U_{sh} . For a quasi-perpendicular shock, both d and P_{esp} have a significant increase toward a large U_{sh} . The drop of d is still caused by the lack of reflection when β_1 approaches unity. The rapid increase of P_{esp} at a large U_{sh} leads to the abrupt growth of γ .

Based on the above results, we find that a steep particle spectrum is expected for a quasi-perpendicular shock with both large α_1 and large U_{sh} , that is, a large β_1 . In Fig. 4, we present γ as a function of β_1 for the four cases shown in Figs. 2 and 3. When a large β_1 ($\gtrsim 0.8$) can be reached, different cases converge toward a steep spectrum with a large γ .

4. STEEP SYNCHROTRON SPECTRA OF RADIO TDES

Particles are accelerated at the shocks induced by TDE outflow-CNM interaction. Because of the combination of a large outflow velocity (Matsumoto & Piran 2021) and a large shock obliquity (see Section 2), the condition of a large β_1 is satisfied. Naturally, we expect a steep particle energy spectrum (Section 3). The spectral index s of synchrotron emission from accelerated electrons is related to γ by $s = (\gamma - 1)/2$. For a quasi-parallel shock in the small β_1 regime, there is $\gamma \approx 2$ and thus $s \approx 0.5$. A steeper particle spectrum at a large β_1 should lead to a steeper synchrotron spectrum.

We collect a number of TDEs with delayed radio flares and available measurements on s from the literature (see Table 1), and we use their estimated outflow velocity as U_{sh} . Note that the uncertainty range of U_{sh} can be large, depending on the assumed outflow geometry (e.g., ASASSN-14li, Alexander et al. 2016), outflow launching time, and CNM density profile (e.g., iPTF 16fnl, Horesh et al. 2021). As expected, their synchrotron spectra are steep, with s significantly larger than 0.5. In Fig. 5, we compare the observations with the

theoretical expectation for a quasi-perpendicular shock. The theoretical curve is taken from XL22. It corresponds to the particle spectral index of a quasi-perpendicular shock with a range of obliquities $[\alpha_{1,\text{max}} - \delta\alpha_1, \alpha_{1,\text{max}}]$, where $\alpha_{1,\text{max}}$ is the maximal obliquity for a subluminal shock, and $\delta\alpha_1$ is the obliquity variation induced by small magnetic fluctuations. We have

$$\gamma = 1 - \frac{\ln(1 - \overline{P_{\text{esp}}})}{\ln(1 + \overline{d})}, \quad (6)$$

where $\overline{\dots}$ denotes obliquity average over the range $[\alpha_{1,\text{max}} - \delta\alpha_1, \alpha_{1,\text{max}}]$. We see that toward a large U_{sh} in the large β_1 regime, s rapidly rises with increasing U_{sh} . At a larger $\delta\alpha_1$, s grows more gradually, with a weaker dependence on U_{sh} .

As a comparison, we also present the observational results of extragalactic young supernova remnants (SNRs), including SN 1987A, SN 1993J, and a number of Type Ib/c SNe (see Bell et al. 2011 and references therein) in Fig. 5. We see a remarkable similarity between the two populations in terms of their fast but non-relativistic outflows and steep radio synchrotron spectra. We note that an alternative explanation for steep synchrotron spectra of young SNRs was discussed in, e.g., Maeda 2013. The similarity between the distribution of common non-relativistic outflows and rare relativistic jets in TDEs and that of common Type Ib/c SNe and rare long-duration gamma-ray bursts was earlier suggested in Alexander et al. (2016). Our results indicate that steep synchrotron spectra can be generally seen for shock acceleration associated with non-relativistic outflows in transient phenomena.

5. DISCUSSION

Observations suggest the existence of cloud-like objects around Sgr A* (e.g., Gillessen et al. 2012). When a TDE outflow interacts with the inhomogeneous CNM and interstellar medium, the turbulence induced by density inhomogeneities can amplify both pre- and post-shock magnetic fields via the turbulent dynamo (Giacalone & Jokipii 2007; Beresnyak et al. 2009; Drury & Downes 2012; del Valle et al. 2016; Xu & Lazarian 2017). The density spectrum measured in the inhomogeneous interstellar medium is frequently much shallower than the Kolmogorov spectrum, and characterized by small-scale high density contrasts (e.g., Xu & Zhang 2016, 2017, 2020). Compared to the shock propagation in a homogeneous medium with a Kolmogorov density spectrum (e.g., Inoue et al. 2013; Ji et al. 2016), the interaction of shocks with density fluctuations with a non-Kolmogorov shallow density spectrum leads to more significant corrugation of the shock surface and amplification of turbulent magnetic fields (Hu et al. in prep). Due to both shock corrugation and turbulent dynamo, a range of shock obliquities is expected, depending on the spectral distribution and density contrast of upstream density fluctuations. In the immediate vicinity of the corrugated shock surface, the magnetic field orientations aligned with the shock surface are preferentially seen, irrespective of the original shock obliquity (Inoue et al. 2013; Hu et al. in prep). Because of the additional SDA induced by shock compression of magnetic fields and the

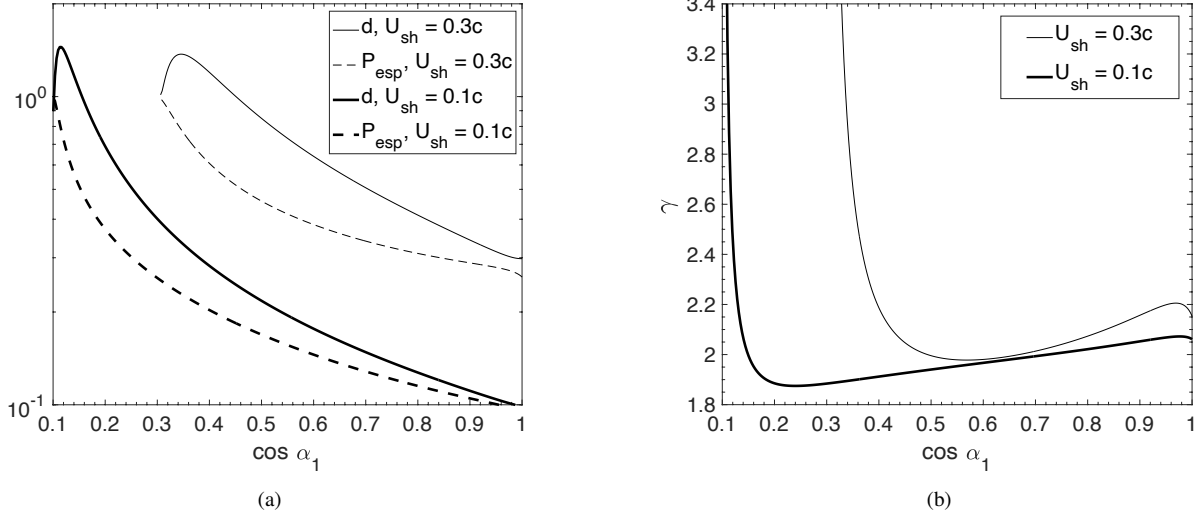


Figure 2. Obliquity (α_1) dependence of d , P_{esp} in (a) and γ in (b) for sub-relativistic shocks.

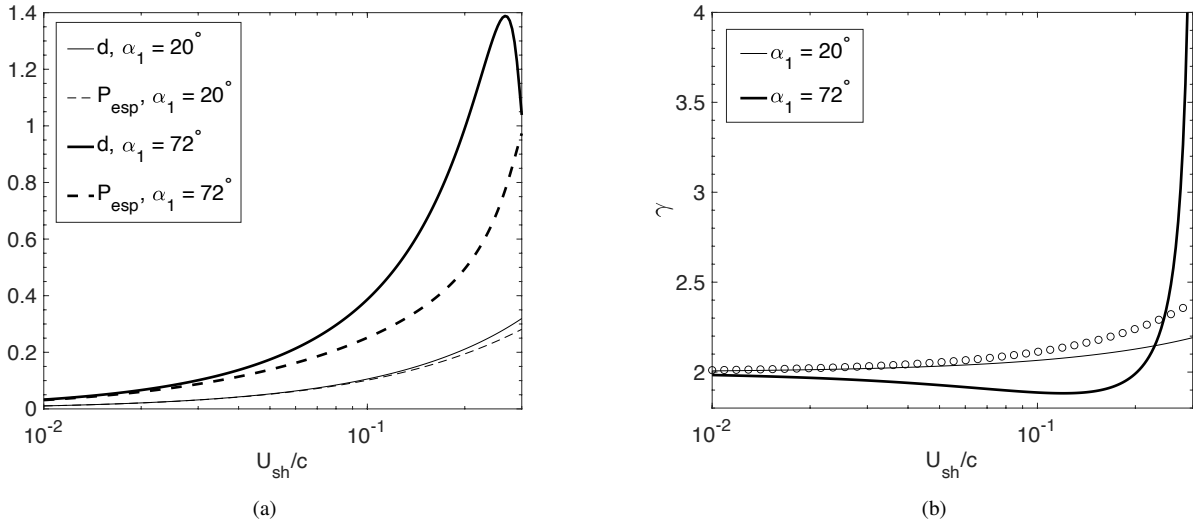


Figure 3. U_{sh} dependence of d , P_{esp} in (a) and γ in (b) for quasi-parallel ($\alpha_1 = 20^\circ$) and quasi-perpendicular ($\alpha_1 = 72^\circ$) shocks. Circles in (b) represent the approximate result given by Eq. (3).

Table 1. Outflow velocity and synchrotron spectral index of radio TDEs

	XMMSL1 J0740-85 (1)	CNSS J0019+00 (2)	ASASSN-14li (3)	AT2019dsg (4)	iPTF 16fnl (5)
U_{sh} [km s $^{-1}$]	10^4	1.5×10^4	$1.2 \times 10^4 - 3.6 \times 10^4$	2.1×10^4	$1.8 \times 10^4 (4.7 \times 10^4)$
s	0.7	1.15	1	0.85	1

(1) Alexander et al. (2017); (2) Anderson et al. (2020); (3) Alexander et al. (2016); (4) Cendes et al. (2021); (5) Horesh et al. (2021).

The lower and upper limits on U_{sh} for ASASSN-14li correspond to spherical and conical outflow geometries. The two values of U_{sh} for iPTF 16fnl correspond to different outflow launching time and CNM density profiles.

suppressed diffusion of particles in the direction perpendicular to the magnetic field (Xu & Yan 2013), a highly oblique shock has a much higher acceleration efficiency than a quasi-

parallel shock and thus tends to dominate the particle acceleration given a complex magnetic field configuration and var-

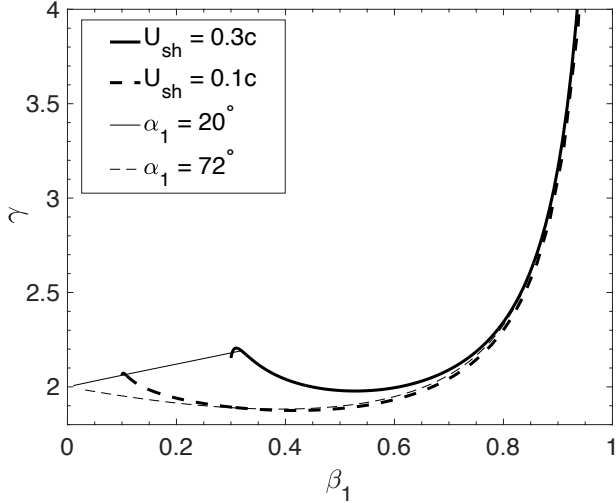


Figure 4. β_1 dependence of γ for the four cases presented in Figs. 2 and 3. Note that different symbols are used here.

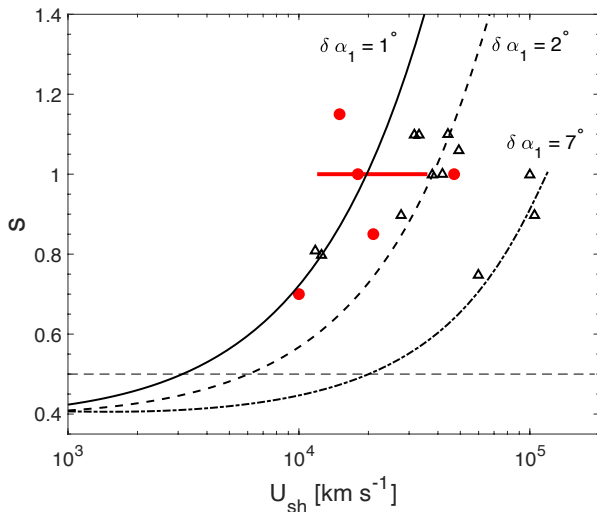


Figure 5. Radio synchrotron spectral index versus shock velocity for TDE outflows (red circles, see Table 1 for the references) and extragalactic SNRs (triangles, see the references in Bell et al. (2011)). The red line corresponds to ASASSN-14li with a range of U_{sh} . The three curves are taken from XL22. They represent the theoretical expectation for a quasi-perpendicular shock with a small obliquity variation $\delta\alpha_1$ caused by magnetic fluctuations. The horizontal dashed line marks $s = 0.5$ for a parallel shock.

ious shock obliquities (Jokipii 1987; Decker 1988; Fulbright & Reynolds 1990; XL22).

TDEs have been suggested as candidates for producing high-energy protons and neutrinos (Murase et al. 2020b), which is also supported by recently reported neutrino events associated with TDEs (e.g., Stein et al. 2021; Reusch et al. 2021; van Velzen et al. 2021). However, with a steep spec-

trum of high-energy protons, it would be difficult for TDE outflows to account for the observed PeV neutrinos (Wu et al. 2021). It suggests that in addition to the shock obliquity, other physical ingredients, e.g., cosmic ray diffusion and feedback, may affect the acceleration of energetic protons. Alternatively, the neutrino production sites can be accretion disks (e.g., Murase et al. 2020a) or jets (e.g., Winter & Lu-nardini 2021).

6. CONCLUSIONS

To understand the origin of delayed TDE radio flares detected in recently years, we study the particle acceleration at the (bow) shocks driven by TDE non-relativistic outflows. In the presence of toroidal magnetic fields in the CNM, these shocks are likely to have large obliquities.

Quasi-perpendicular shocks are intrinsically different from quasi-parallel shocks. Unlike the “universal” spectral index of particles accelerated at a quasi-parallel shock, a quasi-perpendicular shock has a much larger acceleration efficiency and gives rise to a steep particle energy spectrum at a large shock velocity. We find that the combination of a large shock obliquity and a large shock velocity, i.e., a large β_1 , is the necessary condition for spectral steepening. This condition is naturally satisfied for shocks driven by the interaction of a TDE outflow with the CNM and clouds around the SMBH. Therefore, steep particle spectra and thus steep synchrotron spectra are expected from TDE radio flares.

Our theoretical understanding well explains the currently available measurements on synchrotron spectral slopes of radio TDEs. The synchrotron spectral index can be used to constrain the outflow properties and CNM density (Matsumoto & Piran 2021). Similar slopes of synchrotron spectra are also seen in young extragalactic SNRs with similar shock velocities, indicative of the same acceleration mechanism at quasi-perpendicular shocks driven by non-relativistic outflows associated with transient phenomena.

As non-relativistic outflows can be ubiquitous in TDEs (Alexander et al. 2016), more measurements on synchrotron spectra are expected from the synergy between optical transient surveys and radio followups or blind radio surveys (see a review by Alexander et al. 2020 for current surveys). Current radio observations yielded detections of relatively low-redshift TDEs ($z < 0.05$; van Velzen et al. 2018). Radio non-detections of TDEs can be due to their low-luminosity outflows given the wide range of TDE radio luminosities (Alexander et al. 2020). Next generation VLA (ngVLA) and SKA are expected to provide more synchrotron spectrum measurements for larger samples of TDEs at higher redshifts (Alexander et al. 2020). They will provide further tests of our theoretical finding on the steep spectrum of particles accelerated by TDE outflows.

ACKNOWLEDGMENTS

S.X. thanks Alex Lazarian, Bing Zhang, Wenbin Lu, James Stone, and Suvi Gezari for helpful discussion. S.X. also thanks the anonymous referee for helpful comments. S.X. acknowledges the support for this work provided by NASA through the NASA Hubble Fellowship grant # HST-HF2-51473.001-A awarded by the Space Telescope Science Institute, which is operated by the Association of Universities for Research in Astronomy, Incorporated, under NASA contract NAS5-26555.

Software: MATLAB (MATLAB 2021)

APPENDIX

Here we provide the expressions of d_r , d_{12} , d_{21} , P_r , and P_{12} , which were originally introduced in Ostrowski (1988). Their detailed derivation can be found in XL22.

The fractional energy gain in the process of reflection (“x” = “r”), transmission from upstream to downstream (“x” = “12”), and transmission from downstream to upstream (“x” = “21”) is

$$d_x = \frac{\int V_{rel} \left(\frac{E_f}{E_0} - 1 \right) d\mu}{S_x}. \quad (1)$$

E_f/E_0 is the ratio of particle energies after and before a shock encounter. It has expressions

$$\left(\frac{E_f}{E_0} \right)_r = \Gamma_1^2 (1 + 2\beta_1\mu + \beta_1^2) \quad (2)$$

for reflection,

$$\left(\frac{E_f}{E_0} \right)_{12} = \Gamma_2 \Gamma_1 \left(1 + \beta_1\mu - \beta_2 \sqrt{(1 + \beta_1\mu)^2 - \frac{1}{b} \frac{1 - \mu^2}{\Gamma_1^2}} \right) \quad (3)$$

for transmission from upstream to downstream, and

$$\left(\frac{E_f}{E_0} \right)_{21} = \Gamma_1 \Gamma_2 \left(1 + \beta_2\mu + \beta_1 \sqrt{(1 + \beta_2\mu)^2 - b \frac{1 - \mu^2}{\Gamma_2^2}} \right) \quad (4)$$

for transmission from downstream to upstream, where Γ_i is the Lorentz factor corresponding to β_i , μ is the cosine of particle pitch angle, $b = B_1/B_2$, and B_i is the magnetic field strength. The weight function in Eq. (1) is

$$V_{rel,1} = \frac{\mu \cos \alpha_1 + \frac{U_1}{c}}{1 + \frac{U_1 \mu \cos \alpha_1}{c}}, \quad V_{rel,2} = \frac{\mu \cos \alpha_2 + \frac{U_2}{c}}{1 + \frac{U_2 \mu \cos \alpha_2}{c}} \quad (5)$$

in the upstream and downstream regions, respectively, and

$$S_x = \int V_{rel} d\mu. \quad (6)$$

The range of μ for the integral is

$$-\beta_1 < \mu < \frac{\sqrt{1-b} - \beta_1}{1 - \beta_1 \sqrt{1-b}} \quad (7)$$

for reflection,

$$\frac{\sqrt{1-b} - \beta_1}{1 - \beta_1 \sqrt{1-b}} < \mu < 1 \quad (8)$$

for transmission from upstream to downstream, and

$$-1 < \mu < -\beta_2 \quad (9)$$

for transmission from downstream to upstream.

The probabilities of reflection and transmission from upstream to downstream are

$$P_r = \frac{S_r}{S_{12} + S_r}, \quad P_{12} = \frac{S_{12}}{S_{12} + S_r}. \quad (10)$$

REFERENCES

- Alexander, K. D., Berger, E., Guillochon, J., Zauderer, B. A., & Williams, P. K. G. 2016, *ApJL*, 819, L25, doi: [10.3847/2041-8205/819/2/L25](https://doi.org/10.3847/2041-8205/819/2/L25)
- Alexander, K. D., van Velzen, S., Horesh, A., & Zauderer, B. A. 2020, *SSRv*, 216, 81, doi: [10.1007/s11214-020-00702-w](https://doi.org/10.1007/s11214-020-00702-w)
- Alexander, K. D., Wieringa, M. H., Berger, E., Saxton, R. D., & Komossa, S. 2017, *ApJ*, 837, 153, doi: [10.3847/1538-4357/aa6192](https://doi.org/10.3847/1538-4357/aa6192)
- Anderson, M. M., Mooley, K. P., Hallinan, G., et al. 2020, *ApJ*, 903, 116, doi: [10.3847/1538-4357/abb94b](https://doi.org/10.3847/1538-4357/abb94b)
- Armstrong, T. P., Pesses, M. E., & Decker, R. B. 1985, Washington DC American Geophysical Union Geophysical Monograph Series, 35, 271, doi: [10.1029/GM035p0271](https://doi.org/10.1029/GM035p0271)
- Ball, L., & Melrose, D. B. 2001, *PASA*, 18, 361, doi: [10.1071/AS01047](https://doi.org/10.1071/AS01047)
- Bell, A. R. 1978, *MNRAS*, 182, 147, doi: [10.1093/mnras/182.2.147](https://doi.org/10.1093/mnras/182.2.147)
- . 2004, *MNRAS*, 353, 550, doi: [10.1111/j.1365-2966.2004.08097.x](https://doi.org/10.1111/j.1365-2966.2004.08097.x)
- Bell, A. R., Schure, K. M., & Reville, B. 2011, *MNRAS*, 418, 1208, doi: [10.1111/j.1365-2966.2011.19571.x](https://doi.org/10.1111/j.1365-2966.2011.19571.x)
- Beresnyak, A., Jones, T. W., & Lazarian, A. 2009, *ApJ*, 707, 1541, doi: [10.1088/0004-637X/707/2/1541](https://doi.org/10.1088/0004-637X/707/2/1541)
- Bonanno, A., & Urpin, V. 2007, *A&A*, 473, 701, doi: [10.1051/0004-6361:20077726](https://doi.org/10.1051/0004-6361:20077726)
- Burdiak, G. C., Lebedev, S. V., Bland, S. N., et al. 2017, *Physics of Plasmas*, 24, 072713, doi: [10.1063/1.4993187](https://doi.org/10.1063/1.4993187)
- Cendes, Y., Alexander, K. D., Berger, E., et al. 2021, *ApJ*, 919, 127, doi: [10.3847/1538-4357/ac110a](https://doi.org/10.3847/1538-4357/ac110a)
- Christopher, M. H., Scoville, N. Z., Stolovy, S. R., & Yun, M. S. 2005, *ApJ*, 622, 346, doi: [10.1086/427911](https://doi.org/10.1086/427911)
- Ciurlo, A., Campbell, R. D., Morris, M. R., et al. 2020, *Nature*, 577, 337, doi: [10.1038/s41586-019-1883-y](https://doi.org/10.1038/s41586-019-1883-y)
- Decker, R. B. 1988, *SSRv*, 48, 195, doi: [10.1007/BF00226009](https://doi.org/10.1007/BF00226009)
- Decker, R. B., & Vlahos, L. 1986, *ApJ*, 306, 710, doi: [10.1086/164381](https://doi.org/10.1086/164381)
- del Valle, M. V., Lazarian, A., & Santos-Lima, R. 2016, *MNRAS*, 458, 1645, doi: [10.1093/mnras/stw340](https://doi.org/10.1093/mnras/stw340)
- Drury, L. O., & Downes, T. P. 2012, *MNRAS*, 427, 2308, doi: [10.1111/j.1365-2966.2012.22106.x](https://doi.org/10.1111/j.1365-2966.2012.22106.x)
- Fulbright, M. S., & Reynolds, S. P. 1990, *ApJ*, 357, 591, doi: [10.1086/168947](https://doi.org/10.1086/168947)
- Giacalone, J., & Jokipii, J. R. 2007, *ApJL*, 663, L41, doi: [10.1086/519994](https://doi.org/10.1086/519994)
- Gillessen, S., Genzel, R., Fritz, T. K., et al. 2012, *Nature*, 481, 51, doi: [10.1038/nature10652](https://doi.org/10.1038/nature10652)
- Guo, F., Giacalone, J., & Zhao, L. 2021, *Frontiers in Astronomy and Space Sciences*, 8, 27, doi: [10.3389/fspas.2021.644354](https://doi.org/10.3389/fspas.2021.644354)
- Horesh, A., Sfaradi, I., Fender, R., et al. 2021, *ApJL*, 920, L5, doi: [10.3847/2041-8213/ac25fe](https://doi.org/10.3847/2041-8213/ac25fe)
- Hu, Y., Lazarian, A., Beck, R., & Xu, S. 2022a, arXiv:2206.05423, arXiv:2206.05423. <https://arxiv.org/abs/2206.05423>
- Hu, Y., Lazarian, A., & Wang, Q. D. 2022b, *MNRAS*, 511, 829, doi: [10.1093/mnras/stac159](https://doi.org/10.1093/mnras/stac159)
- Inoue, T., Shimoda, J., Ohira, Y., & Yamazaki, R. 2013, *ApJL*, 772, L20, doi: [10.1088/2041-8205/772/2/L20](https://doi.org/10.1088/2041-8205/772/2/L20)
- Ji (), S., Oh, S. P., Ruszkowski, M., & Markevitch, M. 2016, *MNRAS*, 463, 3989, doi: [10.1093/mnras/stw2320](https://doi.org/10.1093/mnras/stw2320)
- Jokipii, J. R. 1982, *ApJ*, 255, 716, doi: [10.1086/159870](https://doi.org/10.1086/159870)
- . 1987, *ApJ*, 313, 842, doi: [10.1086/165022](https://doi.org/10.1086/165022)
- Kirk, J. G., & Heavens, A. F. 1989, *MNRAS*, 239, 995, doi: [10.1093/mnras/239.3.995](https://doi.org/10.1093/mnras/239.3.995)
- Maeda, K. 2013, *ApJL*, 762, L24, doi: [10.1088/2041-8205/762/2/L24](https://doi.org/10.1088/2041-8205/762/2/L24)
- MATLAB. 2021, MATLAB and Statistics Toolbox Release 2021b (Natick, Massachusetts: The MathWorks Inc.)
- Matsumoto, T., & Piran, T. 2021, *MNRAS*, 507, 4196, doi: [10.1093/mnras/stab2418](https://doi.org/10.1093/mnras/stab2418)
- Mou, G., Wang, T., Wang, W., & Yang, J. 2022, *MNRAS*, 510, 3650, doi: [10.1093/mnras/stab3742](https://doi.org/10.1093/mnras/stab3742)
- Murase, K., Kimura, S. S., & Mészáros, P. 2020a, *PhRvL*, 125, 011101, doi: [10.1103/PhysRevLett.125.011101](https://doi.org/10.1103/PhysRevLett.125.011101)
- Murase, K., Kimura, S. S., Zhang, B. T., Oikonomou, F., & Petropoulou, M. 2020b, *ApJ*, 902, 108, doi: [10.3847/1538-4357/abb3c0](https://doi.org/10.3847/1538-4357/abb3c0)
- Naito, T., & Takahara, F. 1995, *Progress of Theoretical Physics*, 93, 287, doi: [10.1143/PTP.93.287](https://doi.org/10.1143/PTP.93.287)

- Nicastro, F., Senatore, F., Krongold, Y., Mathur, S., & Elvis, M. 2016, *ApJL*, 828, L12, doi: [10.3847/2041-8205/828/1/L12](https://doi.org/10.3847/2041-8205/828/1/L12)
- Ostrowski, M. 1988, *MNRAS*, 233, 257, doi: [10.1093/mnras/233.2.257](https://doi.org/10.1093/mnras/233.2.257)
- Piotrovich, M., Silant'ev, N., Gnedin, Y., Natsvlshvili, T., & Buliga, S. 2017, *NewA*, 51, 65, doi: [10.1016/j.newast.2016.08.004](https://doi.org/10.1016/j.newast.2016.08.004)
- Rees, M. J. 1988, *Nature*, 333, 523, doi: [10.1038/333523a0](https://doi.org/10.1038/333523a0)
- Reusch, S., Stein, R., Kowalski, M., et al. 2021, arXiv:2111.09390, arXiv:2111.09390. <https://arxiv.org/abs/2111.09390>
- Roche, P. F., Lopez-Rodriguez, E., Telesco, C. M., Schödel, R., & Packham, C. 2018, *MNRAS*, 476, 235, doi: [10.1093/mnras/sty129](https://doi.org/10.1093/mnras/sty129)
- Saxton, R., Komossa, S., Auchettl, K., & Jonker, P. G. 2020, *SSRv*, 216, 85, doi: [10.1007/s11214-020-00708-4](https://doi.org/10.1007/s11214-020-00708-4)
- Silant'ev, N. A., Gnedin, Y. N., Buliga, S. D., Piotrovich, M. Y., & Natsvlshvili, T. M. 2013, *Astrophysical Bulletin*, 68, 14, doi: [10.1134/S1990341313010021](https://doi.org/10.1134/S1990341313010021)
- Sonnerup, B. U. Ö. 1969, *J. Geophys. Res.*, 74, 1301, doi: [10.1029/JA074i005p01301](https://doi.org/10.1029/JA074i005p01301)
- Stein, R., Velzen, S. v., Kowalski, M., et al. 2021, *Nature Astronomy*, 5, 510, doi: [10.1038/s41550-020-01295-8](https://doi.org/10.1038/s41550-020-01295-8)
- van Velzen, S., Bower, G. C., & Metzger, B. D. 2018, in *Astronomical Society of the Pacific Conference Series*, Vol. 517, *Science with a Next Generation Very Large Array*, ed. E. Murphy, 737. <https://arxiv.org/abs/1810.06677>
- van Velzen, S., Holloien, T. W. S., Onori, F., Hung, T., & Arcavi, I. 2020, *SSRv*, 216, 124, doi: [10.1007/s11214-020-00753-z](https://doi.org/10.1007/s11214-020-00753-z)
- van Velzen, S., Stein, R., Gilfanov, M., et al. 2021, arXiv:2111.09391, arXiv:2111.09391. <https://arxiv.org/abs/2111.09391>
- West, J. L., Safi-Harb, S., & Ferrand, G. 2017, *A&A*, 597, A121, doi: [10.1051/0004-6361/201628079](https://doi.org/10.1051/0004-6361/201628079)
- Winter, W., & Lunardini, C. 2021, *Nature Astronomy*, 5, 472, doi: [10.1038/s41550-021-01305-3](https://doi.org/10.1038/s41550-021-01305-3)
- Wu, C. S. 1984, *J. Geophys. Res.*, 89, 8857, doi: [10.1029/JA089iA10p08857](https://doi.org/10.1029/JA089iA10p08857)
- Wu, H.-J., Mou, G.-B., Wang, K., Wang, W., & Li, Z. 2021, arXiv:2112.01748, arXiv:2112.01748. <https://arxiv.org/abs/2112.01748>
- Xu, S., & Lazarian, A. 2017, *ApJ*, 850, 126, doi: [10.3847/1538-4357/aa956b](https://doi.org/10.3847/1538-4357/aa956b)
- . 2022, *ApJ*, 925, 48, doi: [10.3847/1538-4357/ac3824](https://doi.org/10.3847/1538-4357/ac3824)
- Xu, S., & Yan, H. 2013, *ApJ*, 779, 140, doi: [10.1088/0004-637X/779/2/140](https://doi.org/10.1088/0004-637X/779/2/140)
- Xu, S., & Zhang, B. 2016, *ApJ*, 824, 113, doi: [10.3847/0004-637X/824/2/113](https://doi.org/10.3847/0004-637X/824/2/113)
- . 2017, *ApJ*, 835, 2, doi: [10.3847/1538-4357/835/1/2](https://doi.org/10.3847/1538-4357/835/1/2)
- . 2020, *ApJ*, 905, 159, doi: [10.3847/1538-4357/abc69f](https://doi.org/10.3847/1538-4357/abc69f)